Technical Physics, 2022, Vol. 67, No. 11

15

Comparison of Back-Scattering and Forward-Scattering Methods in Short Range Microwave Imaging Systems

© *V.V. Razevig,*[1] *A.S. Bugaev,*[2] *S.I. Ivashov*[1]

[1] Bauman Moscow State Technical University,
Moscow, Russia
[2] Moscow Institute of Physics and Technology (National Research University),
Dolgoprudny, Moscow Region, Russia
E-mail: vrazevig@rslab.ru

Received June 30, 2022
Revised July 26, 2022
Accepted July 27, 2022

Microwave imaging technique allows obtaining images of hidden objects in structures and media using microwaves. Usually in short-range microwave imaging systems, the back-scattered signal is used, when a combined transmit-receive antenna scans over a plane, forming a two-dimensional synthesized aperture, while the signal reflected from the object of observation is recorded, as a result of which a microwave hologram of the object is formed. The second option involves registering the forward-scattered signal, when the transmitting and receiving antennas are located on opposite sides of the object and scan synchronously. The purpose of this work is a theoretical and experimental comparison of these two sounding options, identifying the advantages and disadvantages of each option, taking into account the features that arise when solving various problems of microwave imaging.

Keywords: microwave holography, mivrowave image, back-scattered signal, forward-scattered signal, range resolution.

DOI: 10.21883/TP.2022.11.55184.173-22

Introduction

Radio vision technology allows using radio waves scattered by objects to determine their position and shape, including when the objects are in an optically opaque environment, but relatively transparent in the radio range. This technology has various applications, such as: non-destructive inspection of structures and materials [1–4]; detection of prohibited items concealed under human clothing [5,6]; visualization of internal structure of human tissues and organs in medicine [7,8]; detection of people behind obstacles [9]. Characteristics of objects are determined by the so-called radar images (radio images), the process of obtaining which consists in the registration of a complex radio hologram of the object and its subsequent recovery. Radio holograms are registered by irradiating the object with a coherent signal using one or a number of transmitting elements distributed in space, and measuring the complex amplitude of the signal scattered by the object using a set of distributed receiving elements.

Often, short-range microwave systems use a single transceiver antenna that scans flat within a given survey area. Scanning is done either by the operator's hand [1], or by the electromechanical scanner 3,4. Such a construction of the antenna system (AS) is monostatic, in which only the principle of „on reflection" can be realized.

In long-range radar systems (RS), the bistatic principle of radar construction, when the transmitting and receiving antennas are on opposite sides of the object of observation, has proven itself well. Such systems use the aperture shadow inversion radar synthesis method, with which it is possible to recover the profile function of the object's shadow silhouette and its shadow spectral portrait [10,11]. The advantage of this construction is that when observing the scattered „forward" field, there is a sharp increase in the effective scattering surface of objects [10], almost independent of the counter-radar cloaking measures [12].

Therefore, it was decided to devote the present work to the study of the „principle„ in short-range microwave systems. The theoretical and experimental comparison of the monostatic and bistatic„luminate" AS configurations is performed in this article. Radio vision systems using a continuous signal with a stepped frequency shift are investigated.

A literature search revealed not many works devoted to short-range microwave systems, working „at lumen", for example, [7,13]. The closest to the present work „luminate" configuration of the antenna system is considered in [7], but it does not compare the options „on reflection" and „at lumen". The [13] proposes a method of obtaining good range resolution, but it requires a multistatic configuration of the antenna system.

1. Theoretical background

Consider the geometry of a microwave system operating „on reflection", with a single receiving and transmitting

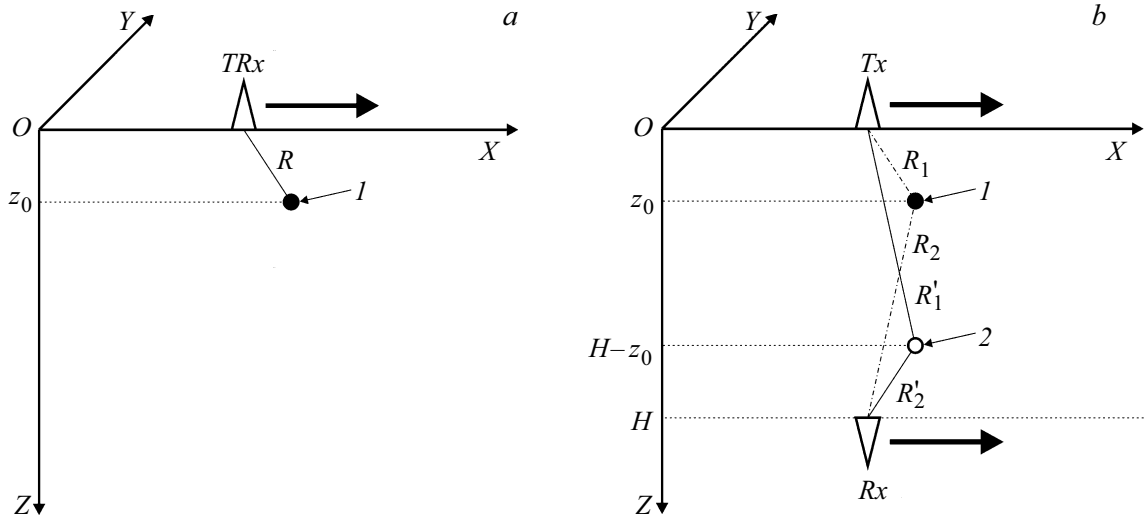

Figure 1. Modifications of microwave systems: *a* — reflective, *b* — at lumen; *1* — true object, *2* — imaginary object.

antenna (TRx), Fig. 1, *a*. The antenna scans in the plane $z = 0$, at each node of the two-dimensional equidistant grid emits a continuous signal with a step change in frequency and at each frequency registers the signal reflected from the object. In the figure, the current direction of antenna movement is shown by an arrow. The object to be probed is an omnidirectional point scatterer located in a perfectly homogeneous medium.

In radio vision systems, the main information about the probed object is the phase overrun during signal propagation on the path „transmitting antenna–object–receiving antenna" [5]. In this configuration, the phase overrun is proportional to twice the distance from the antenna to the object:

$$\Delta\phi(f) = \frac{2\pi f\sqrt{\varepsilon_E}}{c}\,2R, \qquad (1)$$

where c — speed of light, ε_E — permittivity of the medium in which the object being probed is located.

Changing the distance R from the receiving and transmitting AC to the object when scanning the AC in the plane of registration of the radio hologram entails a change in phase overruns, including taking into account the change in frequencies. Therefore, the system working on reflection is able to determine the distance to the sensed object and to resolve objects located at different distances from the sensing plane.

The geometry of the microwave system operating „on the luminate" is shown in Fig. 1, *b*. During scanning, the transmitting (Tx) and receiving (Rx) antennas move synchronously. In this case, the phase overrun depends on the combined distance R_1 (from the transmitting antenna to the object) and R_2 (from the object to the receiving antenna):

$$\Delta\phi(f) = \frac{2\pi f\sqrt{\varepsilon_E}}{c}\,(R_1 + R_2), \qquad (2)$$

In this case, z_0 has little effect on $R_1 + R_2$, especially if the transmitting and receiving antennas during scanning are positioned so that the object is on the line between them or close to it. In addition, for any object located in the plane $z = z_0$, there is an imaginary object located in the plane $z = H - z_0$, where H — the distance between the transmitting and receiving antennas, such that $R_1 + R_2 = R'_1 + R'_2$ at any antenna position during a scan. Here R'_1 — the distance from the transmitting antenna to the imaginary object, R'_2 — the distance from the imaginary object to the receiving antenna. Therefore, it can be assumed that the range resolution will be worse when working at lumen than when working in the reflected light.

Further, we will check this hypothesis by computer simulation, but first we will focus on the method of recovery of radio holograms.

2. Method of radio hologram recovery

Let us introduce a contrast function describing the distribution of the object's electrical properties with respect to its environment [8]:

$$\chi(\mathbf{r}') = \frac{\varepsilon(\mathbf{r}') - \varepsilon_E}{\varepsilon_E}, \qquad (3)$$

where $\varepsilon(\mathbf{r}')$ — the object permittivity at the point $\mathbf{r}' = [x', y', z']^T$ (T — denotes transpose), the medium permittivity.

Radio hologram recovery methods are used to calculate the contrast distribution function over the recovered volume by processing the recorded radio hologram. When displaying the result of recovery, you can visualize the three-dimensional volume of the recovered data as a whole, and build its sections with different planes. Further , both options will be given.

In this work, we will use the inverse projection [14,15] method for recovery, according to which, when „works in reflection“ the contrast function at a point in space with coordinates (x', y', z') can be calculated by the formula

$$\chi(x', y', z') = \sum_{f=f_{\min}}^{f_{\max}} \sum_{x=-S_x/2}^{S_x/2} \sum_{y=-S_y/2}^{S_y/2} E(f, x, y) \times \exp\left(jk2\sqrt{(x'-x)^2 + (y'-y)^2 + (z')^2}\right), \quad (4)$$

where $E(f, x, y)$ — value of the radio hologram recorded at frequency f at the location of the antenna at the coordinates $(x, y, 0)$; $k = 2\pi f\sqrt{\varepsilon_E}/c$ — wave number; $f_{\min}$ and $f_{\max}$ — range of frequency change of probing signal; S_x and S_y — dimensions of radio hologram registration area on corresponding axes, j — imaginary unit. When recovering, the frequency step is equal to the step of the probing signal with frequency step switching. Steps in coordinates X and Y are determined by the characteristics of the scanning system, for best results the distance between adjacent samples should not exceed a quarter of the wavelength [5].

When „works at lumen“ the formula for recovery is as follows:

$$\chi(x', y', z') = \sum_{f=f_{\min}}^{f_{\max}} \sum_{x=-S_x/2}^{S_x/2} \sum_{y=-S_y/2}^{S_y/2} (E(f, x, y) \times \exp\left(jk\left[\sqrt{(x'-x)^2 + (y'-y)^2 + (z')^2}\right] + \sqrt{(x'-x)^2 + (y'-y)^2 + (z'-H)^2}\right). \quad (5)$$

This assumes that the transmitting antenna moves in the $z = 0$ plane and the receiving antenna — in the $z = H$ plane.

3. Computer modeling

The parameters of the computational experiments were as follows:

- frequency range 15–24 GHz in steps of $\Delta f = 250$ MHz (37 frequencies);
- dimensions of the radio logging area $S_x = S_y = 300$ mm;
- step between samples 3 mm on both axes;
- The distance between the antennas along the axis Z in the „luminate option“ $H = 170$ mm.

In the first computational experiment, two omnidirectional point scatterers with coordinates $(-30, 0, 30)$ and $(30, 0, 70)$ mm served as objects. The option of „operation on reflection“ was simulated. The radio hologram was calculated according to the formula

$$E(f, x, y) = E_0\sigma \sum_{i=1}^{N} \left(\frac{G(f, \theta_i, \varphi_i)}{R_i}\right)^2 \exp[-jk2R_i], \quad (6)$$

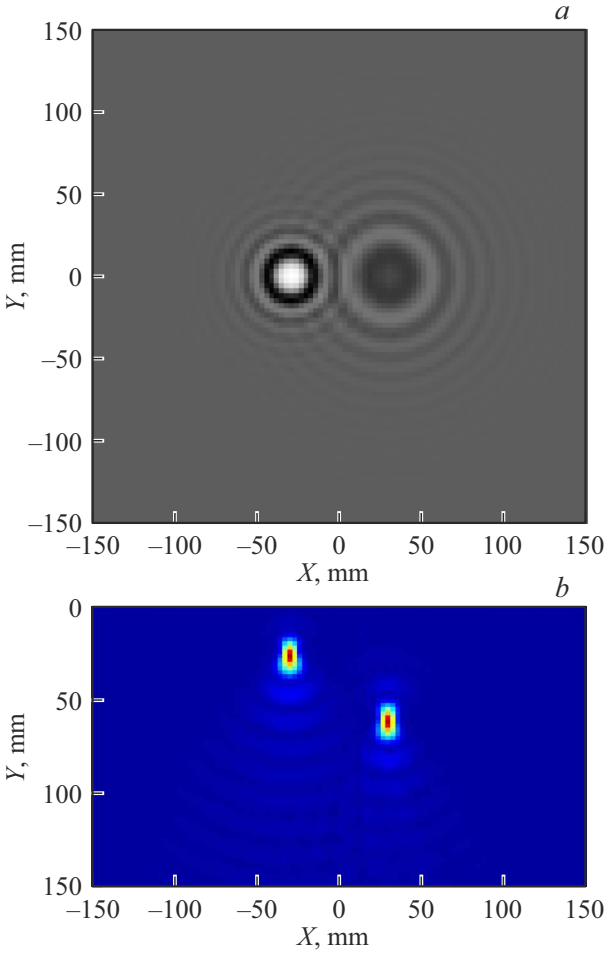

Figure 2. Simulation results of the option „on reflection“: *a* — radio hologram, *b* — result of its recovery.

where E_0 — transmitter excitation amplitude; $\sigma = 1$ — effective scattering area of the point scatterer, entered in the formula to respect the dimensionality; N — number of point scatterers; $R_i = \sqrt{(x - x_i)^2 + (y - y_i)^2 + z_i^2}$ — distance from the current position of the transceiver antenna to ith scatterer with coordinates (x_i, y_i, z_i); $k = \frac{2\pi f\sqrt{\varepsilon_E}}{c}$ — wave number; ε_E — permittivity of medium; $G(f, \theta_i, \varphi_i)$ — antenna directional pattern at frequency f; θ_i and φ_i — the azimuthal and polar angles between the normal to the plane and the direction from the current antenna position to the ith scatterer. The horn antenna radio hologram, which was used in the physical experiments, was calculated in advance using the FEKO electrodynamic modeling program and recorded in a file.

Note, that when „works on reflection“ the multifrequency signal with the parameters specified at the beginning of the section has range resolution $\delta r = c/(2\Delta F) = 1.7$ cm and a single-valued range interval $\delta R = c/(2\Delta F) = 60$ cm.

Fig. 2 shows the radio hologram calculated by the formula (6) (its real part at a frequency 20 GHz is shown) and the results of its recovery — the microwave image built

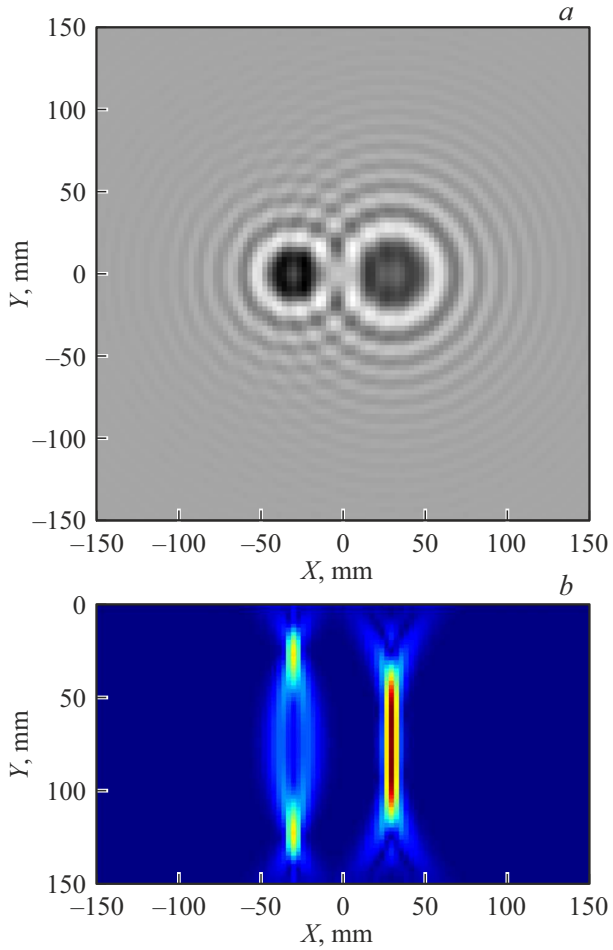

Figure 3. The results of the simulation of the option „at lumen“: *a* — radio hologram, *b* — result of its recovery.

in the vertical plane $y = 0$. The radio image demonstrates that the reflection radio system is capable of determining the spatial position of an object both in the plane of the microwave hologram registration and in the range.

In the second computational experiment, the option „at lumen“ was simulated for the same point scatterers. To calculate the radio hologram we used the formula

$$E(f, x, y) = E_0\sigma \sum_{i=1}^{N} \frac{G(f, \theta_{1,i}\varphi_{1,i})G(f, \theta_{2,i}\varphi_{2,i})}{R_{1,i}R_{2,i}} \times \exp[-jk(R_{1,i} + R_{2,i})], \quad (7)$$

where $R_{1,i} = \sqrt{(x - x_i)^2 + (y - y_i)^2 + z_i^2}$ — the distance from the current transmitting antenna position to the ith scatterer;$R_{2,i} = \sqrt{(x - x_i)^2 + (y - y_i)^2 + (H - z_i)^2}$ — the distance from ith scatterer to the current position of the receiving antenna; $\theta_{1,i}, \varphi_{1,i}$ and $\theta_{2,i}, \varphi_{2,i}$ — angles related to the transmitting and receiving antennas, respectively.

The simulation results are shown in Table 3. The obtained microwave image (Fig. 3, *b*) confirmed the preliminary theoretical reasoning, and also revealed interesting points. If the object is located close to the antenna (in this experiment, the left scatterer at a distance of $z = 30$ mm), then, as expected, there is an imaginary twin for it in the radio image, located at a distance of $170-30 = 40$ mm. In this case, it is impossible to determine which of the responses corresponds to the true position of the object. A object farther away from the antenna (right scatterer at $z = 70$ mm) is not localized in the radio image at all by the range, „smearing“ almost the entire range.

Let us explain the reason for this with the help of geometric constructions. Let's first analyze the „option of reflection“. For simplicity, consider planar geometry at $y = 0$ (Fig. 1, *a*). Let the point scatterer have coordinates $(x_0, 0, z_0)$. Knowing the phase arrival of the reflected signal at the current position of the antenna $(x_A, 0, 0)$ during its movement along the axis x allows the distance to the scatterer R[1]. Consequently, with measurements at one antenna position, the position of the scatterer can be said to lie on a circle of radius R centered at $(x_A, 0, 0)$. As you move the antenna, each position of the antenna gives a new circle, with the result that the position of the scatterer can be defined as the point of intersection of all the circles. Let's illustrate this with Fig. 4, *a*, where the circles are plotted for the 11 positions of the antenna, which are shown by the black circles. The constructions are made for two scatterers with coordinates, as before, $(-30, 0, 30)$ and $(30, 0, 70)$ mm, their positions are shown as white circles with a black border. The circles for the different diffusers are shown with different lines (solid and dashed). You can see that the circles intersect at different angles, resulting in a good localization of both scatterers. We can also see that in the option „on reflection“ there are also imaginary objects (in Fig. 4, *a* the left imaginary scatterer is visible, and the right one also exists, but it is not in the mapped area), but they fall into another half-space (in the area of negative values Z), so they do not interfere with determining the true position of the object.

Let's move on to the option „at lumen“. In this case, the phase overrun measured at one position of the transmitting antenna with coordinates $(x_A, 0, 0)$ and the receiving antenna with coordinates $(x_A, 0, H)$ can determine the total distance $R_1 + R_2$ (Fig. 1, *b*). The points for which $R_1 + R_2 = \text{const}$ lie on an ellipse centered at $(x_A, 0, H/2)$, the length of the major axis is $R_1 + R_2$, and the length of the minor axis is — $\sqrt{(R_1 + R_2)^2 - H^2}$. The geometric constructions are shown in Fig. 4, *b*, from which we can see that the scatterer located at a smaller range (30 mm) is localized, and for it there is a double in the same half-space. The ellipses corresponding to the longer-range scatterer (70 mm) intersect at sharp angles, almost touching each other, so it is almost impossible to localize this scatterer by range.

[1] Note that the phase arrival can only be uniquely measured within $\pm 180°$, although the true value of the phase arrival at the considered frequencies and at the analyzed geometry can reach hundreds of radians, see formula (1), so measurements at several frequencies are needed to unambiguously determine the distance

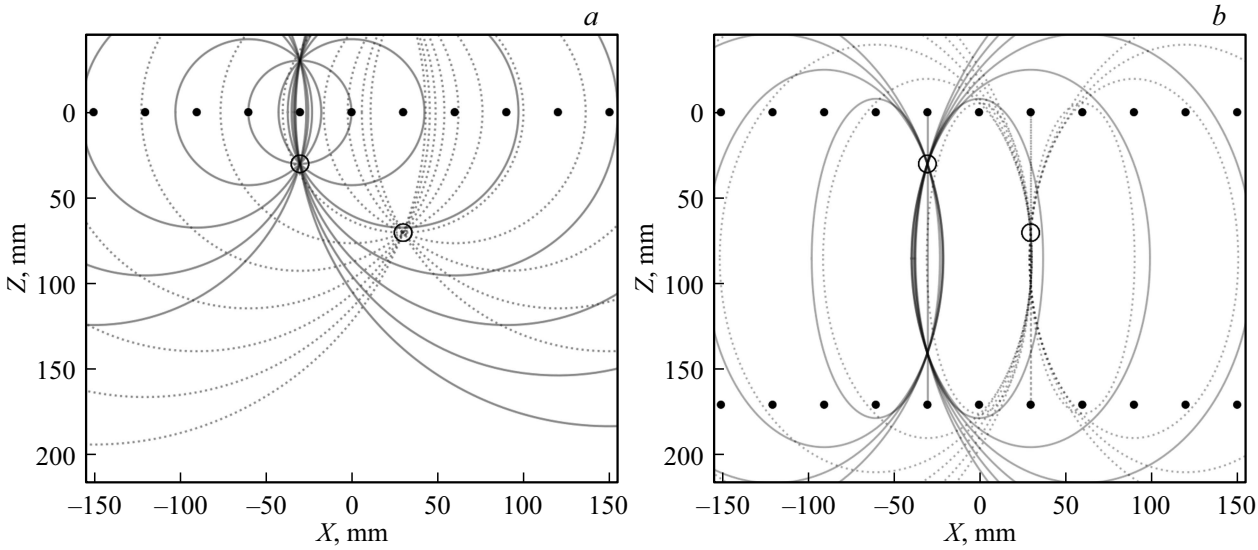

Figure 4. Illustration of object localization: *a* — for reflection, *b* — at lumen.

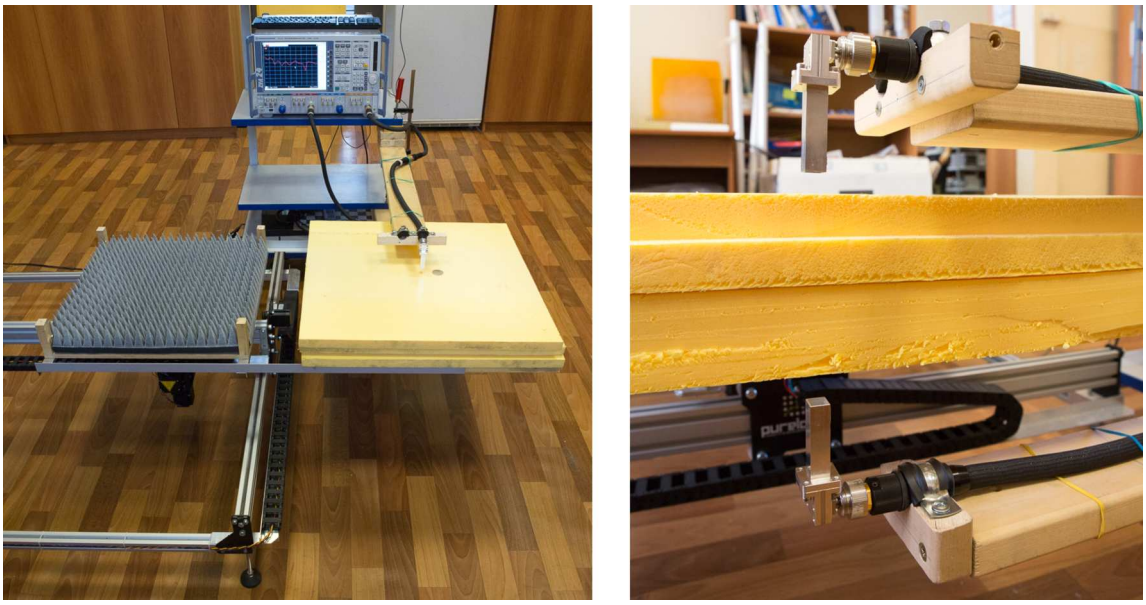

Figure 5. Installation for recording radio holograms.

4. Experiment

The experiments were carried out with a radar system consisting of a vector circuit analyzer (VAC) and a two-dimensional electromechanical scanner. The system uses the principle of inverse aperture synthesis: the antenna system is stationary, and the scanner moves past it the object being surveyed.

In the original setup, the scanner carriage [16] had a mounting table (MC) with supports in the corners, on which a polyurethane foam sheet (or several sheets) was placed to hold the survey objects. A radio-absorbing material was placed between the sheet and the MS to prevent reflections from the metal scanner rails. In such a design, it was impossible to install a second antenna from below in order to implement the option of probing „at lumen. Therefore, the outriggers made of aluminum angle were attached to the MC, and the polyurethane foam sheets were placed on them (Fig. 5, left). The antenna connected to the second port of the VAC was mounted at the top, and the antenna connected to the first port — at the bottom (Fig. 5, right).

Pre-calibration of the antenna-feeder tracts was performed using the method described in [17].

During the experiment, all *S*-parameters of the two-port system were simultaneously recorded. In the „reflection„ option, the parameter S_{22} was used (since the

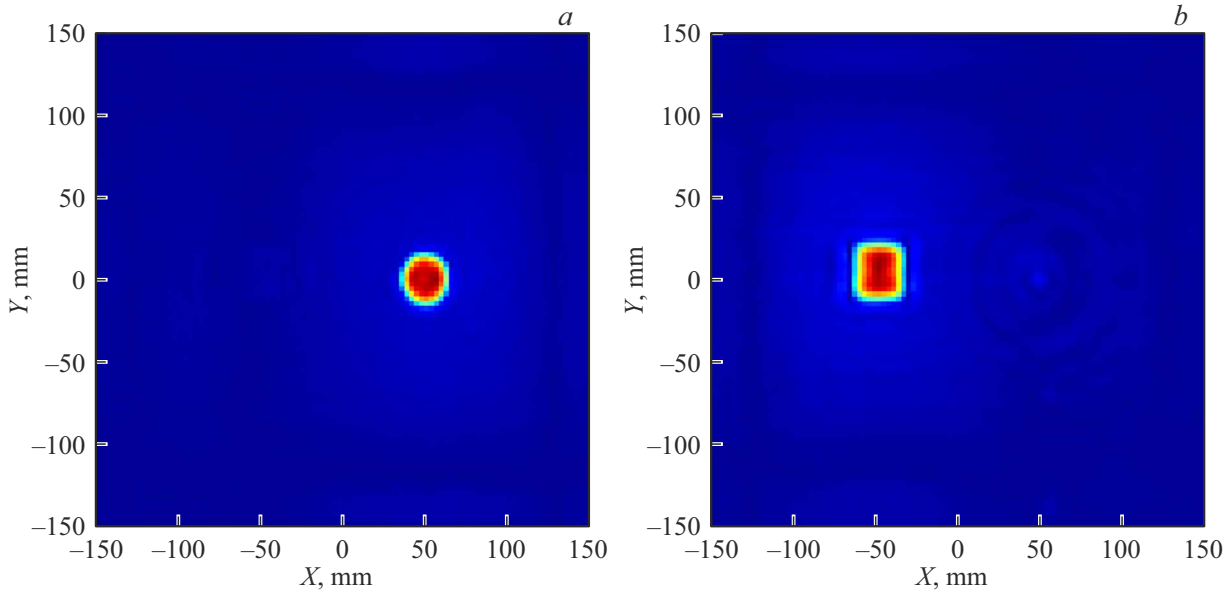

Figure 6. The radio images of the circle and square for the option „on reflection", constructed for different planes, z: *a* - 60, *b* - 110 mm.

antenna connected to port № 2 was placed on top), and in the option at lumen, the parameter S_{21} was used.

The parameters of the physical experiments coincided with the parameters of the computational experiments.

In the first experiment, a metal square with a side of 30 mm was placed on the bottom sheet of polyurethane foam with a thickness of 50 mm, and a metal circle with a diameter of 30 mm was placed on the top sheet. The antennas were placed so that the distance from the bottom antenna to the surface of the bottom sheet was 10 mm. The distance between the antennas, as mentioned above, was 170 mm (it should be noted that the pictures in Fig. 5 were taken at a smaller distance between the antennas). Thus, in the coordinate system shown in Fig. 1, Z-coordinate of the circle was equal to 60 mm, and the square — 110 mm.

The recorded radio holograms are very similar to those obtained by simulation, so we will not give them here to save space. The results of the radio hologram recovery for the option „on reflection" are shown in Fig. 6.

You can see that in each radio image there is only the object that is located in the plane for which the microwave image is constructed. In the radio image in Figure 6, *a* there is not even a trace of the second, more distant object. In the radio image in Fig. 6, *b* there is a faint trace of a circle, which is closer to the upper antenna than the square, and the level of the signal reflected from it is greater. The results of the recovery of the radio hologram for the option „at lumen" are shown in Fig. 7.

In the radio images constructed for the planes $z = 60$ and 110 mm, both objects are present — as already mentioned, each has an image of a true object and an image of an imaginary object located at a different range (the distances in the experiment were chosen so that the imaginary objects fall into the plane of location of the other object). Moreover, in the radio image constructed for the intermediate plane $z = 85$ mm, both objects are also present, but here they are slightly more blurred. This confirms the empirical reasoning and computer simulation results.

The second experiment used a more complex spatially extended object — a metal cross mounted obliquely on a sheet of polyurethane foam (Fig. 8).

The radio holograms recorded during operation at reflection and at lumen are shown in Fig. 9 (the actual parts of the radio holograms at 20 GHz are shown).

Here there is a difference between the radio holograms: in Fig. 9, *a* it is impossible to determine the shape of the object, but intuitively it seems to be tilted [18]; in Figure 9, *b*, by contrast, the shape of the object is clearly visible, but it appears flat.

The results of radio hologram recovery for options „on reflection" and „at lumen" are shown in Figs. 10 and 11, respectively.

For the cross the difference between the two options remains: when using the reflected signal on each radio image there is a fragment of the object, corresponding to the plane of construction of the radio image (with the strobe in the range is determined by the bandwidth of the probing signal), and the passed signal gives „shadow" microwave image of the object, almost independent of the distance to the plane for which it is constructed. It should be noted that when working on reflection, it is also possible to „collect„ the entire spatially distributed on-axis object in a single radio image. To do this, you must apply the method of maximum intensity projection [19], which consists in calculating a three-dimensional array of recovered data, selecting in it for each coordinate (x, y) value with the maximum intensity and assigning it to the corresponding

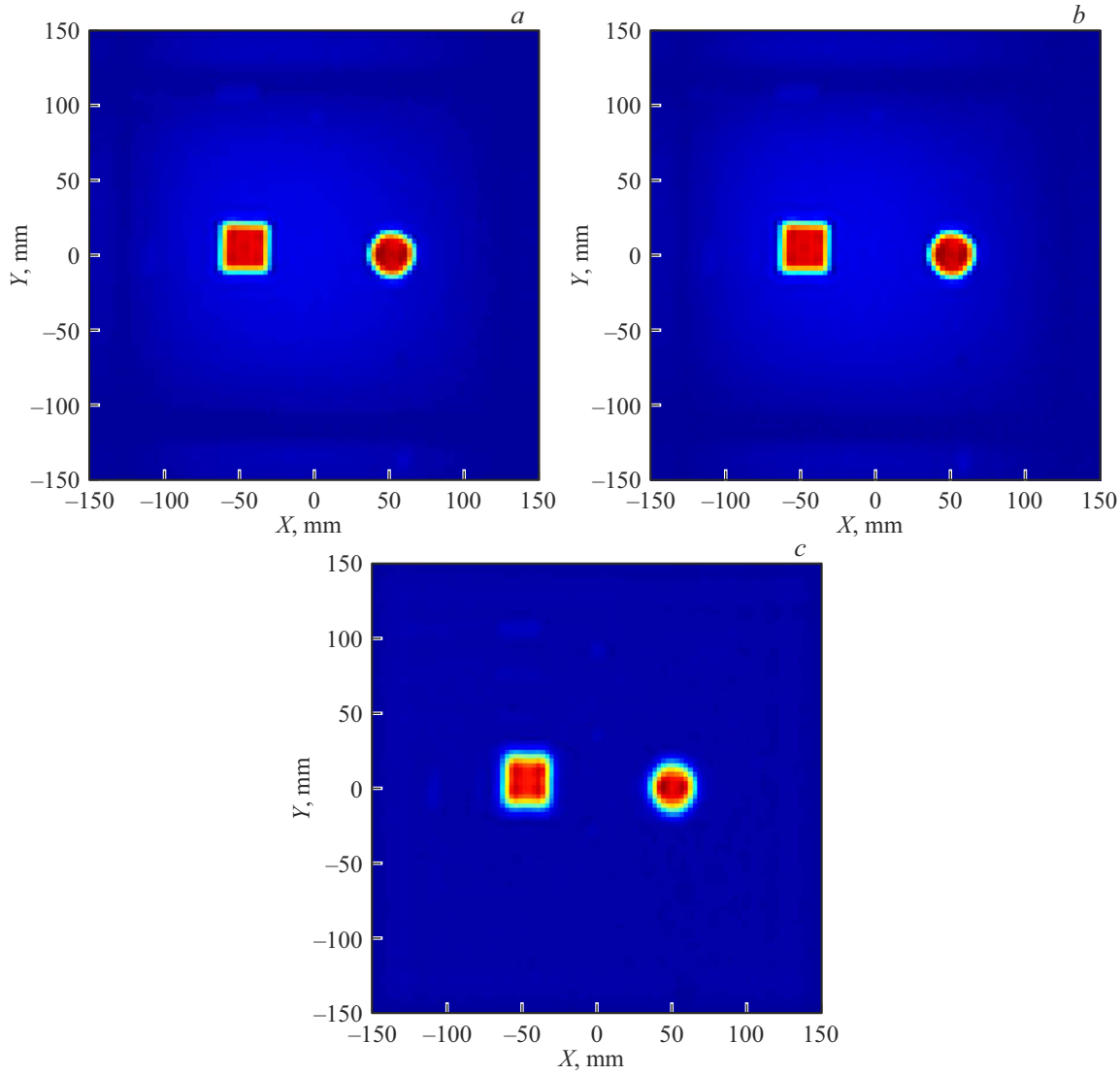

Figure 7. The radio images of the circle and the square for the option „at lumen", plotted for different planes, z: a — 60, b — 110, c — 85 mm.

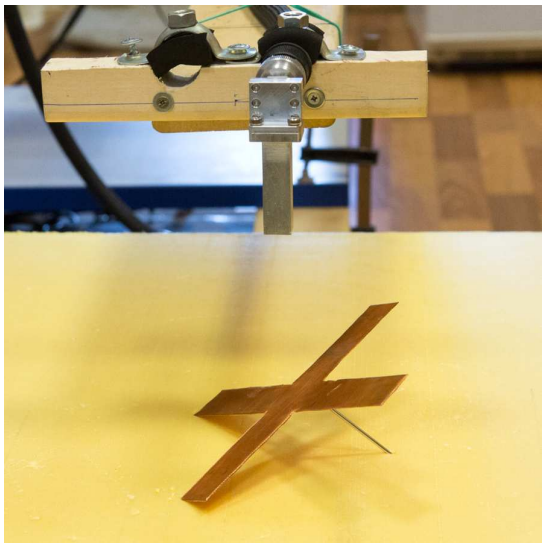

Figure 8. A cross, mounted obliquely.

pixel of the flat radio image:

$$I_{2D}(x, y) = \max_{z}[I_{3D}(x, y, z)], \quad (8)$$

where $I_{3D}(x, y, z)$ — three-dimensional array of recovered data, $I_{2D}(x, y)$ — flat microwave image.

To conclude, in Fig. 12, we present the results of visualization of the three-dimensional array of the recovered data.

In the third experiment, we compare the reflectance and light options of „and„ in the examination of low-contrast objects, such as air cavities in a sheet of polyurethane foam (as opposed to metal objects with good reflectance in the first two experiments). For this purpose, a test sample was prepared with notches of different shapes and depths on its upper surface (Fig. 13). During probing, the sheet with notches was covered with the same sheet, but without

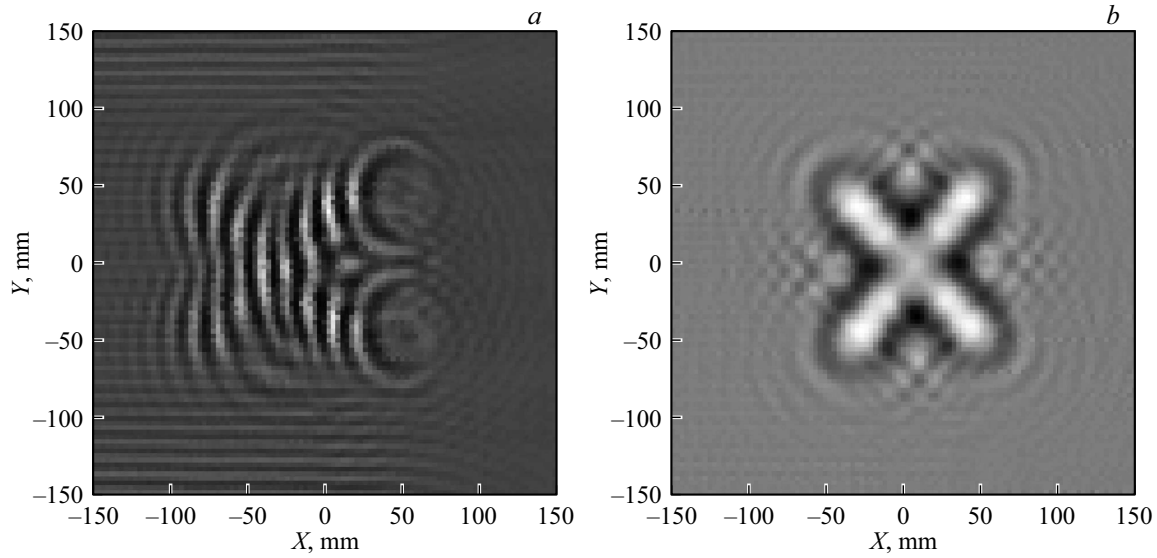

Figure 9. Radio holograms of the oblique cross: *a* — at reflection, *b* — at lumen.

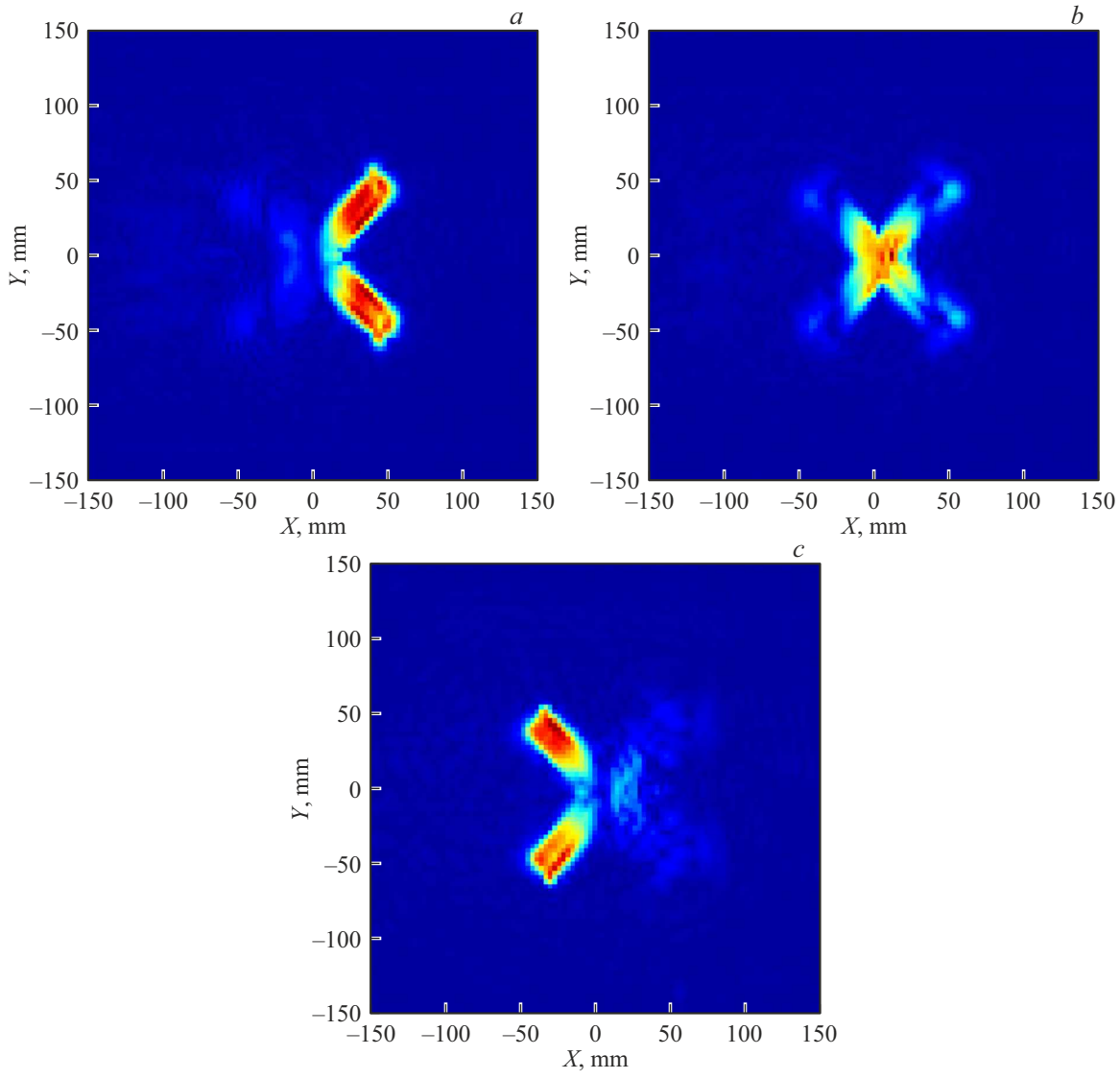

Figure 10. Radio images of the tilted cross for the option „on reflection“, constructed for different planes, *z*: *a* — 60, *b* — 80, *c* — 100 mm.

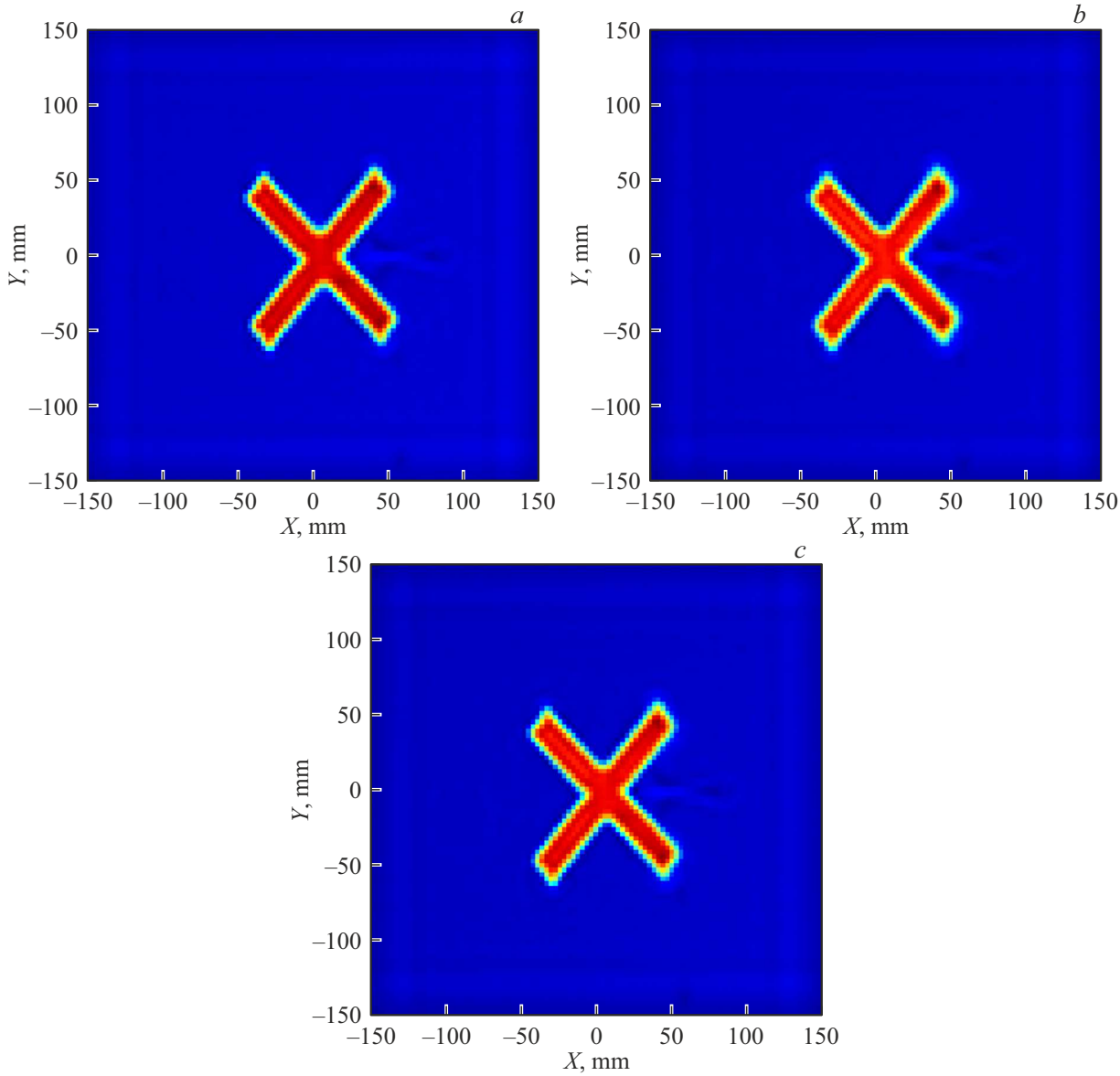

Figure 11. Radio images of the tilted cross for the option „at lumen“, plotted for different planes, z: a — 60, b — 80, c — 100 mm.

notches, thus simulating air cavities in the thickness of the sample.

In Fig. 13, a the white background of the objects corresponds to cutouts with a depth of 2.5−3 mm, and the gray background — with a depth of 9−10 mm. The variation in depth is due to the fact that the cuts were made manually.

In this experiment the parameters were changed: the size of the registration area was equal to 350×300 mm, and the vertical distance between the antennas — 126 mm. The results of the recovery of radio holograms plotted for the two probing options in the plane $z = 60$ mm (distance from the upper antenna to the surface of the sheet with notches) are shown in Fig. 14.

The analysis of the obtained radio images allows us to make the following observations:

- background artifacts are significantly less in the radio image for the case „at lumen“;
- In the radio image, the cavities with a greater thickness (the length along the axis Z) have a greater brightness, so we can assume that the transmission option of „at lumen“ allows us to estimate the thickness of objects [2];
- In the „to reflection“ option there is no relationship between the thickness of the cavity and its brightness in the radio image, on the contrary, the cavities of low thickness (upper left and lower left) have higher brightness than thicker cavities; this is probably due to the fact that in this option the wave reflection occurs mainly from the „environment-canopy“ border closest to the antenna;

[2] An additional experiment with wooden poles of different thickness has not confirmed an unambiguous relationship between the thickness of the object and its brightness in the radio image.

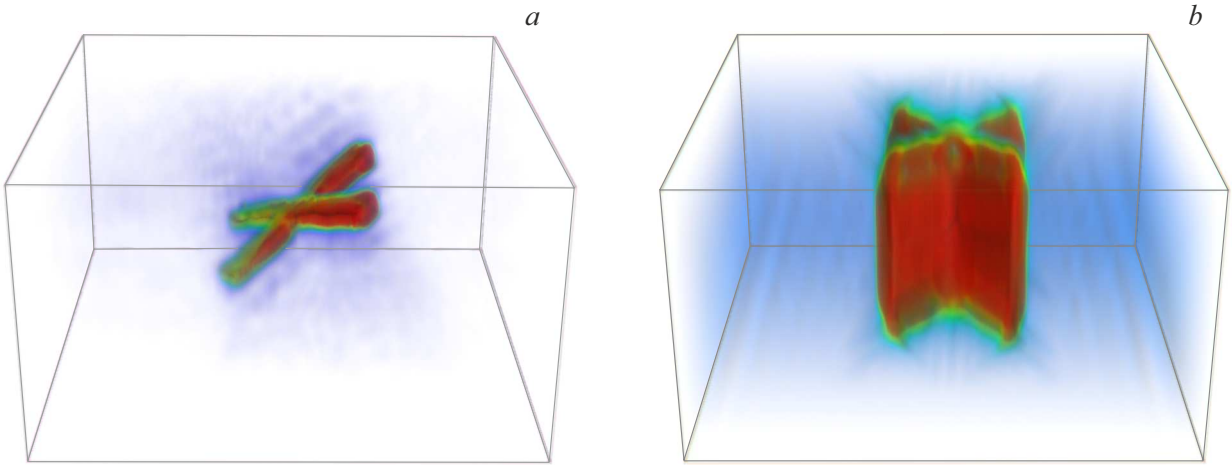

Figure 12. Visualization of the three-dimensional recovered data array for the cross: *a* — at reflection, *b* — at lumen.

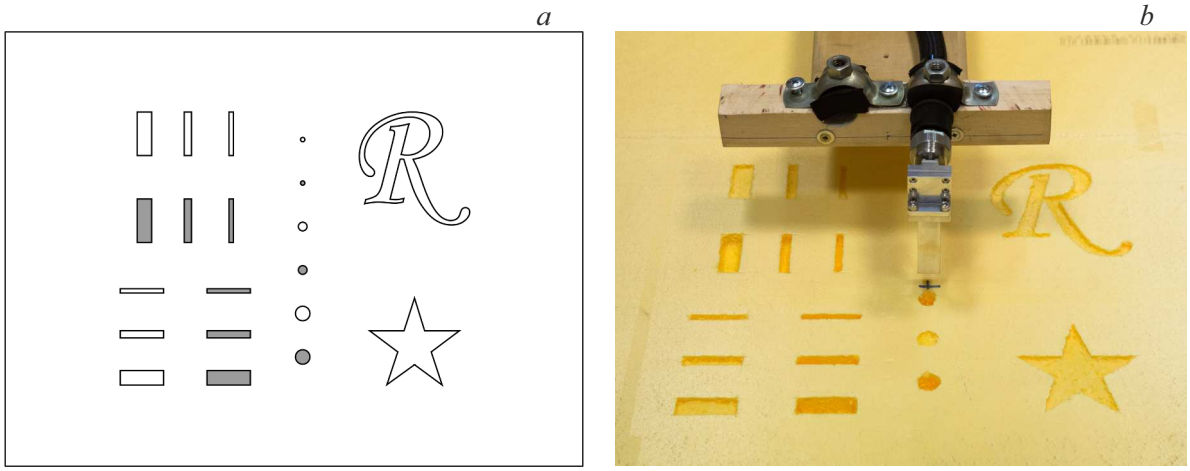

Figure 13. Test pattern: *a* — drawing, *b* — photograph.

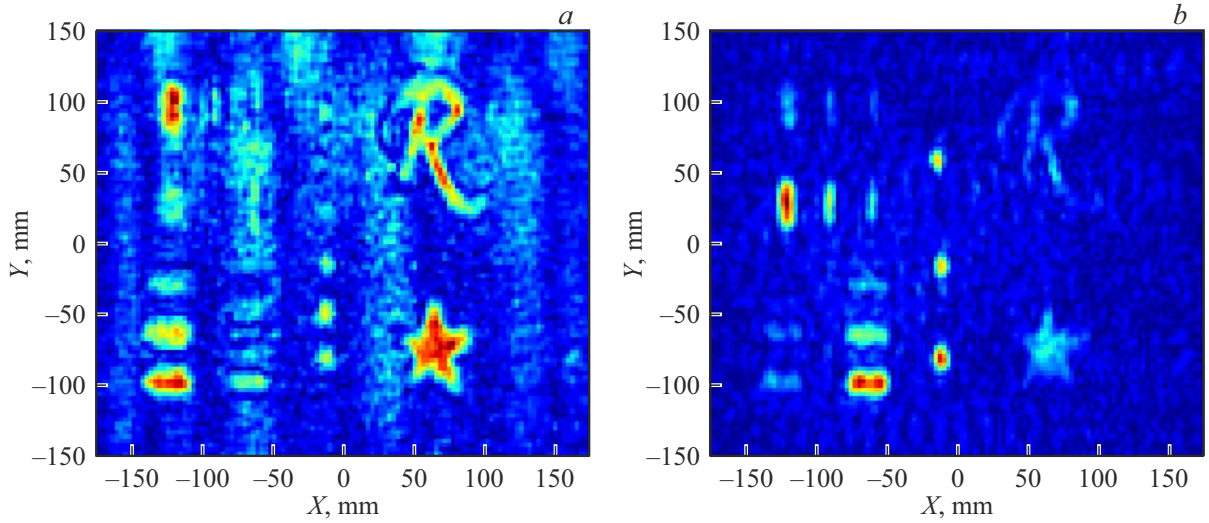

Figure 14. Radio images of a sheet of polyurethane foam with cutouts: *a* — at reflection, *b* — at lumen.

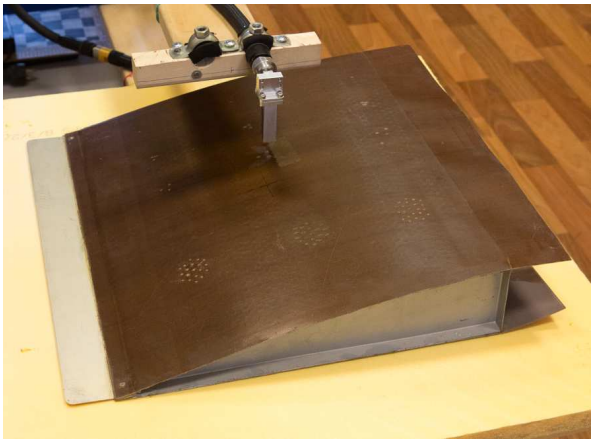

Figure 15. Helicopter blade.

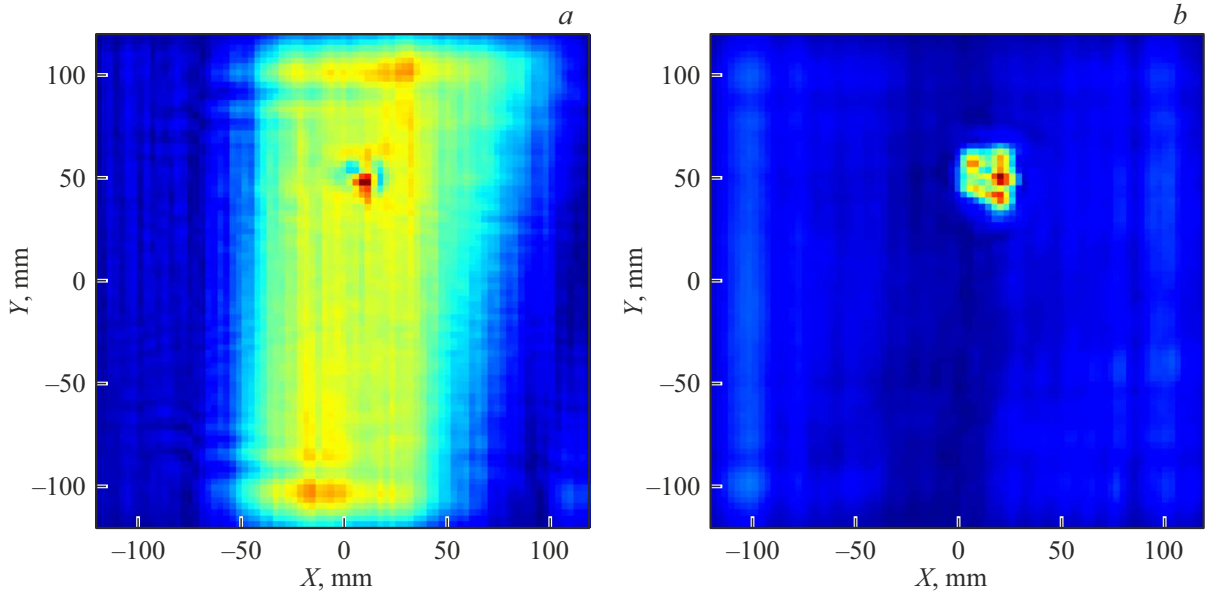

Figure 16. The radio images of the helicopter blade in the water in the honeycomb: *a* — in reflection, *b* — at lumen.

• Smaller thickness cavities are better seen „in the reflective“ option, and thicker ones — „at lumen“ option.

In the final experiment, the two approaches were compared on a fragment of a helicopter blade provided by the Moscow Helicopter Plant named after M.L. Mil (Fig.15). The specimen is made of fiberglass-based composite material and has a honeycomb internal structure with a honeycomb size of about 7.5 mm. A syringe was used to inject 2 ml of water into each of the three adjacent honeycombs. Detection of moisture in helicopter blades made of composite materials is a very topical problem, since its presence leads, firstly, to cracking of blades and loss of bearing capacity in the process of repeated transformation of water into ice and back, and, secondly, to unbalancing of propeller rotor due to the change of blade weight [20].

This experiment is interesting because the upper surface of the sample is not flat. The point is that when examining objects with a flat and/or non-parallel plane of registration of radio holograms upper surface, the distance from the registration plane to the surface at different positions of the antenna is different. Because of this, when „works on the reflection“ a significant contribution to the radio hologram is made by reflections from the surface, which often exceed the level of reflections from internal objects/defects, which prevents their detection and recognition. There are many works devoted to this problem, for example [21–23].

In this experiment, the size of the registration area was 240×240 mm (smaller than the fragment itself so that strong reflections from the metal edges of the sample would not get into the radio hologram), and the vertical distance between the antennas — again 170 mm. The results of recovered of radio holograms, plotted for two options of sounding in the plane $z = 57$ mm (distance from the antenna to the surface of the blade at the point of water injection), are shown in Fig. 16.

It can be seen that the signal reflected from the upper surface of the blade made a significant contribution to the obtained microwave image (Fig. 16, *a*), which makes it difficult to detect water-filled honeycombs on it. When working with „at lumen" the variable thickness of the object has almost no effect on the radio image (the background in Fig. 16, *b* is quite uniform), and the problem area can be identified with greater reliability.

Conclusion

In the work an experimental comparison of two options for constructing a short-range microwave system is performed:

1) The „option on reflection", when a single receiving and transmitting antenna scans the plane, forming a synthesized aperture and registering the reflected signal from the probed object;

2) option of „at transmitting„receiving antennas, which are separated in range, scanning synchronously, registering the passed signal.

The most obvious advantages of the „on reflection" option are that there is no need for two-sided access to the object and the possibility to examine objects restricted on one side by a radio-transparent material, for example, thermal insulation coatings applied on a metal substrate. If we do not take this into account, i.e. consider that the object is permeable to electromagnetic waves and can be accessed from two sides, then we can distinguish the following advantages and disadvantages of each option.

The „reflection„ option has a range resolution determined by the bandwidth of the probing signal. It is possible to localize an object by range and resolve several objects located at different ranges. However, when probing metallic objects, only the position of the surface of the object closest to the antenna can be determined, the reflection from the far boundary is not registered. For dielectric objects in the recorded data reflections from the surface far in relation to the antenna are present, but they are weaker in level, and therefore it is not always possible to determine the position of the far boundary also. Disadvantages of the method appear when examining samples with a flat surface, in the thickness of which the objects/defects to be detected are located. The variable distance from the antenna to the sample surface during scanning causes surface reflections that mask reflections from subsurface objects/defects. To suppress them, you need to use some sort of filtering methods when processing radio holograms.

In the option „at light" the range resolution is generally much worse than in the reflected option, and the farther the object is located from the transmitting (receiving) antenna, the worse the range resolution is. If the distance from the antenna to the object is more than about a quarter of the distance between the antennas, the range resolution practically disappears, and the object is smeared" over all ranges, i.e., when building the radio images in planes parallel to the registration plane, the object is present in all planes, starting from the plane of the object location and beyond. But if in the problem to be solved there is no need to determine the distance to the object, but only to know its coordinates in the plane XOY, this disadvantage turns out to be an advantage: in order to „find" all objects that may be at different distances, it is enough to build a microwave image for the plane lying in the middle between the antennas, while in the option „on reflection" for this you must build radio images for different distances, which requires more time.

A great advantage of the option „on the transmitted light" is the low sensitivity to the variable distance from the detection plane to the surface of samples with a non-flat surface, in the thickness of which the objects/defects to be detected are located.

When examining objects that have the same dielectric properties but different thicknesses, the level of the transmitted signal should probably be related to the thickness of the object. Therefore, we can assume that in the „lumen" option it is possible to determine the thickness of objects, at least relative. The first dedicated experiment did not reveal an unambiguous connection between the thickness of the object and its brightness in the radio image, so additional research is required to confirm the possibility of determining the thickness.

The level of the signal depends on the length of its propagation path. The closer the object is to the antenna, and the closer the object is to the antenna, the more the signal level is to the „transmitted" option, the more the object is located between the antennas: closer to one of the antennas or closer to the middle of the antennas. Therefore, when probing media with high attenuation, for a situation where the sample has a significant thickness and the subsurface object/defect is located close to the surface, the „on reflection" method may have an advantage in terms of the level of the useful signal.

Funding

The study was supported by grants from the Russian Science Foundation № 21-19-00043 (in part to modify the setup to implement the lumen option, conduct experiments, and process the results) and the Russian Foundation for Basic Research № 20-57-46004 (in part to mathematical modeling).

Conflict of interest

The authors declare that they have no conflict of interest.

References

[1] A.V. Zhuravlev, S.I. Ivashov, V.V. Razevig, I.A. Vasiliev, A.S. Bugaev. 7th International Workshop on Advanced Ground Penetrating Radar Nantes, 1–6 (2013). DOI: 10.1109/IWAGPR.2013.6601548

[2] M. Ghasr, Y. Le Pape, D. Scott, R. Zoughi. ACI Mater. J., **112**, 115 (2015). DOI: 10.14359/51686981
[3] L. Capineri, M. Chizh, A. Zhuravlev, V. Razevig, S. Ivashov, P. Falorni. NDT E International, **109**, 102191 (2020). DOI: 10.1016/j.ndteint.2019.102191
[4] S. Kharkovsky, R. Zoughi. IEEE Instrumentation & Measurement Magazine, **10** (2), 26 (2007). DOI: 10.1109/MIM.2007.364985
[5] D.M. Sheen, D.L. McMakin, T.E. Hall. IEEE Transactions on Microwave Theory and Techniques, **49** (9), 1581 (2001).
[6] L. Carrer, A.G. Yarovoy. *The 8th European Conference on Antennas and Propagation* (EuCAP 2014), p. 2786–2790. DOI: 10.1109/EuCAP.2014.6902403
[7] R.K. Amineh, A. Khalatpour, H. Xu, Y. Baskharoun, N.K. Nikolova. Intern. J. Biomed. Imaging, **2012**, Article ID 291494, (2012). DOI: 10.1155/2012/291494.
[8] R. Chandra, I. Balasingham, H. Zhou, R.M. Narayanan. *Medical Microwave Imaging and Analysis, Chapter 19 in Medical Image Analysis and Informatics: Computer-aided Diagnosis and Therapy* (Boca Raton, FL: CRC Press, 2017). ISBN: 978-1-4987-5139-7, p. 451–466.
[9] P.K. Kumar, T.K. Kumar, 2011 International Conference on 3D Imaging (IC3D), 1–5 (2011). DOI: 10.1109/IC3D.2011.6584387
[10] M. Cherniakov (ed.). *Bistatic Radar. Principles and Practice* (Wiley, England, 2007)
[11] V.V. Chapursky. Radiotekhnika, **3**, 52 (2009).
[12] P.Y. Ufimtsev. Proc. IEEE, **84** (12), 1830 (1966).
[13] R.K. Amineh, M. Ravan, J. McCombe, N. K. Nikolova. 2013 IEEE MTT-S International Microwave Symposium Digest (MTT), 1–3 (2013). DOI: 10.1109/MWSYM.2013.6697459
[14] D.L. Mensa. *High Resolution Radar Cross-section Imaging* (Artech House, Norwood, MA, 1991)
[15] A.A. Kuriksha. Radiotekhnika i elektronika, **47** (12), 1484 (2002).
[16] V.V. Razevig, A.S. Bugaev, S.I. Ivashov, A. Kizilay. Electromagnetic Waves and Electronic Systems, **26** (6), 5 (2021). DOI: 10.18127/j15604128-202106-01.EDNXHBVNA
[17] V.V. Razevig, A.V. Zhuravlev, A.S. Bugaev, M.A. Chizh. 2017 Progress in Electromagnetics Research Symposium — Fall (PIERS — FALL), 178–185 (2017). DOI: 10.1109/PIERS-FALL.2017.8293133
[18] L. Capineri, P. Falorni, M. Inagaki, T. Bechtel, V. Razevig, C. Windsor. *Proceedings of the XIII International Conference on Ground Penetrating Radar* (Lecce, Italy, 21–25 June 2010), p. 657–662.
[19] R.H. Hashemi, W.G. Bradley, C.J. Lisanti. *MRI: The Basics* (Wolters Kluwer Health, 2012), ISBN 9781451148718
[20] R.W. Gent, N.P. Dart, J.T. Candsdale. *Aircraft Icing* (Defense Evaluation and Research Agency, Farnborough, Hampshire GU14 OLX, UK, The royal Society, 2000)
[21] Y. Altuncu, I. Akduman, A. Yapar. IEEE Geosci. Remote Sens. Lett., **4** (2), 251 (2007).
[22] M. El-Shenawee. J. Opt. Soc. Amer. A. Opt. Image Sci. Vis., **20** (1), 183 (2003).
[23] X. Zhu, Z. Zhao, W. Yang, Y. Zhang, Z. Nie, Q.-H. Liu. Progr. Electromagn. Res., **117**, 19 (2011).